Applied Catalysis B: Environmental 303 (2022) 120931

Contents lists available at ScienceDirect

Applied Catalysis B: Environmental

journal homepage: www.elsevier.com/locate/apcatb

The role of the surface acidic/basic centers and redox sites on TiO_2 in the photocatalytic CO_2 reduction

Laura Collado [a,b,**], Patricia Reñones [a], Javier Fermoso [c], Fernando Fresno [a], Leoncio Garrido [d], Virginia Pérez-Dieste [e], Carlos Escudero [e], María D. Hernández-Alonso [f], Juan M. Coronado [c,1], David P. Serrano [b,c,**], Víctor A. de la Peña O'Shea [a,*]

[a] Photoactivated Processes Unit, Institute IMDEA Energy, Avda. Ramón de la Sagra 3, 28935 Madrid, Spain
[b] Department of Chemical and Energy Technology, ESCET, Rey Juan Carlos University, c/ Tulipán, 28935 Madrid, Spain
[c] Thermochemical Processes Unit, Institute IMDEA Energy, Avda. Ramón de la Sagra 3, 28935 Madrid, Spain
[d] Institute of Polymer Science and Technology (ICTP-CSIC), c/ Juan de la Cierva 3, 28006 Madrid, Spain
[e] ALBA Synchrotron Light Source, Carrer de la Llum 2–26, Cerdanyola del Vallès, 08290 Barcelona, Spain
[f] Repsol Technology Lab, c/ Agustín de Betancourt s/n, 28935 Madrid, Spain

ARTICLE INFO

Keywords:
Photocatalytic CO_2 reduction
TiO_2 active reaction pathways
Intermediates
In-situ NAP-XPS
In-situ ^{13}C NMR

ABSTRACT

The development of sustainable processes for CO_2 reduction to fuels and chemicals is one of the most important challenges to provide clean energy solutions. The use of sunlight as renewable energy source is an interesting alternative to power the electron transfer required for artificial photosynthesis. Even if redox sites are mainly responsible for this process, other reactive acidic/basic centers also contribute to the overall reaction pathway. However, a full understanding of the CO_2 photoreduction mechanism is still a scientific challenge. In fact, the lack of agreement on standardized comparison criteria leads to a wide distribution of reported productions, even using the same catalyst, which hinders a reliable interpretation. An additional difficulty is ascertaining the origin of carbon-containing products and effect of surface carbon residues, as well as the reaction intermediates and products under real dynamic conditions. To determine the elusive reaction mechanism, we report an interconnected strategy combining in-situ spectroscopies, theoretical studies and catalytic experiments. These studies show that CO_2 photoreduction productions are influenced by the presence of carbon deposits (i.e. organic molecules, carbonates and bicarbonates) over the TiO_2 surface. Most importantly, the acid/base character of the surface and the reaction medium play a key role in the selectivity and deactivation pathways. This TiO_2 deactivation is mainly initiated by the formation of carbonates and peroxo- species, while activity can be partially recovered by a mild acid washing treatment. We anticipate that these findings and methodology enlighten the main shadows still covering the CO_2 reduction mechanism, and, most importantly, provide essential clues for the design of emergent materials and reactions for photo(electro)catalytic energy conversion.

1. Introduction

The continuing rise in atmospheric CO_2 levels has become one of the most enduring problems faced by humankind. Finding sustainable ways to turn CO_2 into valuable products is imperative to mitigate global warming and to provide a long-term solution to the growing energy demand [1–4]. By mimicking nature, the scientific community has devoted great efforts to recycle waste CO_2 into fuels and organic building-blocks using artificial photosynthesis (AP) technologies [5–9]. This promising approach uses solar energy to produce fuels, which are very attractive means for energy storage due to their high specific energy (e.g. 55 $MJ{\cdot}kg^{-1}$ for methane versus less than 1 $MJ{\cdot}kg^{-1}$ for present-day batteries) [10], and for providing a sustainable future energy supply, alternative to conventional fossil fuels [7,8].

The AP process comprises two apparently simple main reactions: the water splitting and the reduction of CO_2. However, in practice CO_2

* Corresponding author.
** Corresponding authors at: Department of Chemical and Energy Technology, ESCET, Rey Juan Carlos University, c/ Tulipán, 28935 Madrid, Spain.
E-mail addresses: laura.collado@imdea.org (L. Collado), david.serrano@imdea.org (D.P. Serrano), victor.delapenya@imdea.org (V.A. de la Peña O'Shea).
[1] Present Address: Instituto de Catálisis y Petroleoquímica, CSIC, Marie Curie, 2, Cantoblanco, 28049 Madrid, Spain

https://doi.org/10.1016/j.apcatb.2021.120931
Received 31 August 2021; Received in revised form 10 November 2021; Accepted 13 November 2021
Available online 17 November 2021

photoreduction with simultaneous H_2O oxidation is a complex and non-selective multi-electron process, that involve different kind of catalysts based on inorganic, organic and hybrid materials [9–13], and usually leads to a large variety of products, mainly hydrocarbons and oxygenates [11]. In addition to redox sites, acidic and basic surface centers play a key role in the reactivity, selectivity and stability of the catalysts used for this reaction. The reactive adsorption of CO_2 on surface acidic or basic sites, together with the presence of hydroxyl groups and oxygen-deficient surfaces, determine the formation of particular reaction intermediates and products in CO_2 photoreduction. Besides, recent works have also reported the effect of surface frustrated Lewis pairs (FLPs) [14–16] on the mechanism responsible for the photocatalytic hydrogenation of CO_2. While important efforts have been made to understand the effect of redox and acidic/basic sites on CO_2 photoreduction, the reaction mechanism has not been completely clarified and many uncertainties remain unsolved.

In addition to active sites, this reaction strongly depends on the catalyst nature (e.g. surface area, oxygen vacancies, etc.) and the operation conditions (e.g. purity of reagents, irradiance, sacrificial agents, detection limit, etc.). Therefore, several factors such as the presence of O_2 traces, adsorbed carbon residues on the catalyst surface, and the existence of more favorable competitive and backward reactions (such as the oxidation of formed products) [17,18] are unpredictable a priori and significantly affect the reported productions (Fig. 1b). In fact, there is much debate in this regard in the literature [19] (reported productions differ by several orders of magnitude even at comparable reaction conditions, see Fig. 1a), thus complicating a reliable interpretation. On one hand, standard terminology for photocatalysis (i.e. photonic efficiency/yield) is not often reported in the literature despite IUPAC recommendations [20] (e.g. less than 10% of CO_2 photoreduction publications and less than 2% using TiO_2, see Table S2) [19]. Thus, the lack of a general agreement on a standardized comparison criterion complicates the fundamental understanding of the overall process, and explains the high dispersion of production yields and hardly comparable data that clearly limit the development of this technology.

Therefore, a deeper mechanistic understanding is crucial to achieve real progress in the development of the AP process, and will directly impact on the advance of CO_2 valorization technologies and of multitude

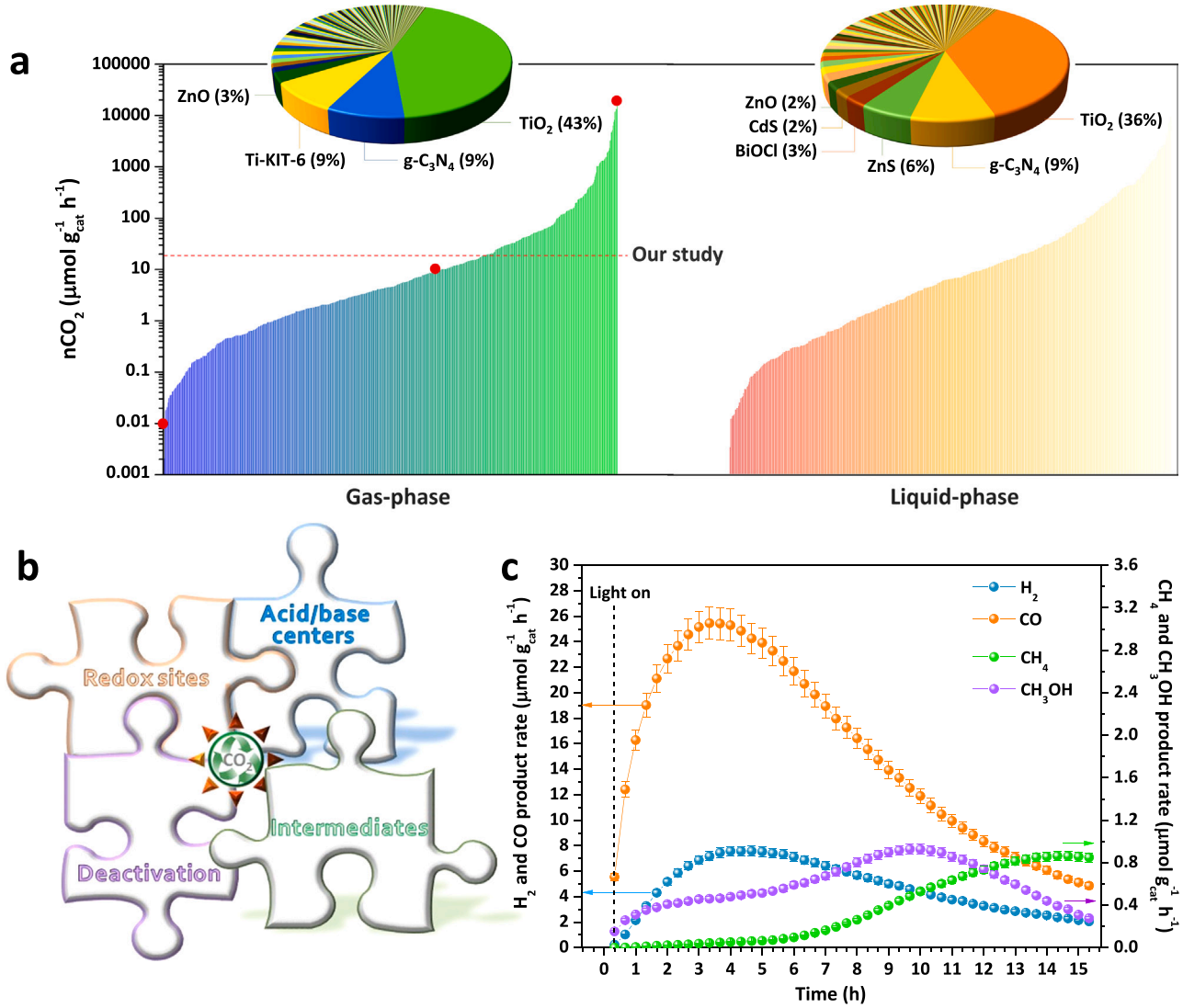

Fig. 1. (a) Literature comparison of CO_2 conversion over TiO_2-based catalysts in reported gas and liquid-phase studies from 1970 to date; nCO_2 stands for total CO_2 converted, which is defined as ∑(mol of carbon products x No. carbons). Data collected from Art Leaf Database (http://www.artleafs.eu/public/home.php), including a total of 4999 entries (56% gas-phase and 44% liquid-phase studies). Points highlighted in red in the gas-phase graph (left side) are summarized in Table S1. Dashed red line represents the nCO_2 value obtained in the present study. Insert pi chart shows percentage of publications by type of catalyst, being TiO_2 the most commonly employed material out of all gas and liquid-phase studies; (b) Uncertain factors to clarify the CO_2 photoreduction process; (c) Product evolution of the photocatalytic reduction of CO_2 with water under UV irradiation ($\lambda = 365$ nm) using TiO_2 (error bars ± 5%).

of light-driven reactions. Over the last years, recognized studies [17,18,21–23] have investigated the CO_2 photoreduction mechanism, providing valuable clues although not yet the overall intricate mechanism. Indeed, this is a complex issue that involves multi electronic reactions occurring at different timescales (i.e. fs-s). The charge dynamics of the process was investigated in our previous studies [24,25], and now we put our focus on the catalysis. Titanium dioxide is the benchmark material for CO_2 reduction mainly because it is available at low price and has been extensively characterized [11,26], which makes it the most suitable candidate for systematic studies. Here, in an effort to further close the gap between idealized and real working conditions, we report a multi-technique study that aims to provide new insights into the surface reactivity of the benchmark TiO_2 (Fig. 1a) in terms of activity, selectivity and stability.

In this work, CO_2 photoreduction has been investigated in a holistic manner by the combination of a series of in-situ spectroscopies, theoretical studies and an extensive number of catalytic reactions under different operational conditions, which allow us to elucidate the nature of the acidic/basic and redox active sites and their decisive role in the reaction mechanism. Besides, here we address some key questions that were still unclear up to date; such as the interference of surface residues that influences a reliable quantification of the CO_2 conversion; the effect of oxygen traces; and the deactivation pathways and regeneration strategies. Further, these findings provide valuable insights for the rational design of novel catalysts with controllable efficiency, selectivity and stability, applicable to other light-mediated reactions.

2. Experimental

2.1. Materials

Anatase-type TiO_2 was obtained from Crystal ACTIV™ (PC500, Lot Number 6293000586), and it was subjected to a thermal treatment at 400 °C for 4 h prior to use to remove possible impurities. A commercial sample was selected in order to minimize the experimental variability and perform systematic measurements with good reproducibility.

2.2. Photocatalytic CO_2 reduction tests

Experiments were conducted in continuous- flow mode in a home-made reaction system (Scheme 1 in Supplementary Material). The powdered catalyst (0.1 g) was deposited on a glass microfiber filter. Illumination was carried out using four 6 W lamps with a maximum emission at 365 nm and an average irradiance of 33.9 Wm^{-2} (measured on top the filter by a Blue-Wave radiometer in the range 330–400 nm). Compressed CO_2 ($\geq$ 99.9999%, Praxair) and water (Milli-Q), were passed through a controlled evaporation and mixing unit, maintaining a molar ratio of 7.25 (CO_2:H_2O). The reaction conditions were set at 2 bar and T = 50–150 °C. In-line gas chromatography (Agilent 7890 A) analyzes were performed to detect the reaction products. The GC is equipped with two separation branches, one equipped with two semicapillary columns (BR-Q Plot and BR-Molesieve 5 A) and one thermal conductivity detector, a flame ionization detector (FID) and a methanizer. The second separation branch consists on a capillary column (CP-Sil 5B) and a second FID. Before starting the experiments, the reactor was first degassed under vacuum and then purged for 1 h using argon (100 mL min^{-1}) to remove any residual organic compounds weakly adsorbed on the surface of the catalyst. Then, the reactor was flushed with the CO_2 and water mixture for 1 h to establish an adsorption–desorption balance at the reaction temperature. Analogously, photocatalytic experiments under argon, argon + H_2O, and CO_2 were performed following the same reaction procedure but changing the feeding gas. Post-reaction treatment was performed by immersing the catalyst filter in an aqueous nitric acid solution (0.1 M) for 30 min. The filter was then washed with distilled water and dried in the oven at 100 °C before reaction tests.

The photonic efficiency (ξ) towards CO was calculated as the ratio between the rate of reaction and the incident photon flux, according to Eq. (1).

$$\xi = \frac{2 \quad dN/dt}{\int_{\lambda_1}^{\lambda_2} q^0_{p,\lambda} dt} \qquad \text{Eq. (1)}$$

where 2 represents the number of electrons involved in the conversion of CO_2 to CO; dN/dt represents the production rate of CO, and $q^0_{p,\lambda}$ is the incident spectral photon flux within a defined wavelength range (ca. 330–400 nm). The superscript 0 (zero) emphasizes that the incident number of photons (prior to absorption) is considered. The incident spectral photon flux was calculated from the lamp emission spectrum (see Scheme 1d in Supplementary Material), recorded with a StellarNet UVNb-50 spectroradiometer connected to an optical fiber.

Isotope tracing experiments were carried out in a 15.6 mL stainless steel reactor with a borosilicate glass window operated in batch mode. After outgassing, $^{13}CO_2$ (Cambridge Isotope Laboratories, Inc., 99.2% ^{13}C, < 1% ^{18}O) and H_2O were introduced in the reactor at 50 °C and 2 bar. After 30 min UV irradiation (four 6 W lamps, fluorescent Philips Actinic, λ_{max} = 365 nm), the gas was analyzed in a quadrupole mass spectrometer (Pfeiffer OMNISTAR).

2.3. General characterization

Carbon content was determined using a THERMO SCIENTIFIC Flash 2000 Elemental Analyzer after sample combustion at 900 °C. Samples weight loss and carbon-products desorption were monitored in a thermobalance TA Instruments SDT Q-600, coupled to an on-line mass spectrometer (Pfeiffer OMNISTAR). Further characterization (N_2 adsorption–desorption isotherms XRD, TEM) can be found in a previous study [24] and is also summarized in Fig. S1.

2.4. Temperature programmed desorption experiment

To identify the acid and basic sites on the TiO_2 surface, temperature programmed desorption (TPD) measurements were carried out using an AUTOCHEM II 2910 instrument (Micromeritics), equipped with a thermal conductivity detector (TCD). For NH_3-TPD tests, the catalyst sample (0.1 g) was degassed under He flow at 350 °C for 30 min, cooled down to three different temperatures (50, 100 and 150 °C) in He flow, and then treated with 5 vol% NH_3/He until the material was saturated at those temperatures. Then, the sample was purged at the same temperature under He flow in order to remove the weakly physisorbed ammonia until only He was detected in the TCD signal. Finally, the NH_3-TPD profile was subsequently recorded increasing the temperature from 50, 100 or 150–550 °C using a ramp rate of 5 °C min^{-1}. A final isotherm at 550 °C of 30 min was added in order to ensure a complete NH_3 desorption. The experimental procedure for CO_2-TPD measurements was similar to that followed for the NH_3-TPD test at 50 °C, but changing the probe molecule to CO_2.

2.5. Theoretical calculations

Theoretical calculations by periodic density functional theory (DFT) were carried out using a 114-atom TiO_2 nanoparticle with anatase structure [27]. Geometry and electronic structure were performed using the projected augmented wave method implemented in Viena ab initio simulation package (VASP) [28,29]. The total energies corresponding to the optimized geometries of all samples were calculated using the spin polarized version of the Perdew−Burke−Ernzerhof (PBE) [30]. The Heyd-Scuseria-Enzerhof hybrid functional (HSE06) [31], with a mixing parameter of 0.325, was used to fit a more accurate energy gap. The cut-off for the kinetic energy of the plane-waves was set to 450 eV to ensure a total energy convergence better than 10^{-4} eV. The cut-off for the kinetic energy of the plane-waves was set to 500 eV to ensure a total

energy and force convergence better than 10^{-4} eV and 0.01 eV/Å^3, respectively.

Theoretical optoelectronic properties of TiO_2 were calculated using time dependent Density Functional Theory (TD-DFT) [32,33] implemented in the software Gaussian 09 [34], employing a CAM-B3LYP functional [35] and using a DGDZVP2 basis set [36,37]. A fixed number of 150 states was selected for a proper comparison between all configurations and models. The interactions between reagents and intermediates with surface sites were explored by molecular dynamics using a hydroxylated TiO_2 nanoparticle (40 nm) and CO_2, H_2O, CO_3^{2-}, HCO_3^- molecules. The system was equilibrated for ~ 10 ps using a 1 fs timestep at 323 K. A Berendsen thermostat controlled the ionic temperature ($dt/\tau = 1/50$).

2.6. In-situ diffuse reflectance infrared fourier transform spectroscopy

Measurements were performed on a Thermo-Nicolet FTIR instrument, which housed a Harrick DRIFTS (diffuse reflectance infrared Fourier transform spectroscopy) reaction cell with three quartz windows, in which the gas stream passed through the powdered sample. Spectra were collected at a resolution of 4 cm^{-1} with 32 co-added scans in the range 650–4000 cm^{-1} using a liquid N_2-cooled MCT detector. A step with argon flow (10 mL min^{-1}) at 50 °C was performed for 1 h, after acquiring a spectrum of the fresh sample in air as background. Then, a 5 sccm flow of 0.1% CO_2 in humid Ar (saturated with water using a thermostated bubbler) was introduced to the cell. Illumination was carried out using a 365 nm LED lamp.

2.7. In-situ Raman

Spectra were recorded using a JASCO NRS-5000/7000 series laser spectrometer equipped with a Linkam CCR1000 in situ cell with a quartz window in which the gas stream passed through the powdered sample. Excitation was performed with a 532 nm laser. The reaction conditions were the same as those used for in situ DRIFTS. Illumination was carried out using a 365 nm LED lamp.

2.8. Near-ambient pressure X-ray photoelectron spectroscopy

A PHOIBOS 150 NAP energy analyzer at the NAPP branch from CIRCE beamline of the ALBA synchrotron light source was used to perform these experiments. The CIRCE beamline is an undulator beamline with a photon energy range 100–2000 eV. In this work, data was acquired with photon energy $h\nu = 900$ eV, using an analyzer pass energy of 10 and 20 eV. The beam spot size at the sample is around 100×90 μm^2 (HxV). Powdered samples were pressed into round disks. Ti 2p NAP-XPS spectra were recorded in UHV and under both dark and illumination conditions. In addition, C 1s and O 1s were acquired in UHV and under a CO_2 and H_2O mixture. NAP-XPS experiments under illumination were performed using a UV LED (Hamamatsu Co.) with a maximum emission centered at 365 nm. The Au 4 $f_{7/2}$ peak at 84.0 eV from a Au foil was taken as energy reference. These studies were performed as follows: ultrapure water (LC–MS CHROMASOLV® grade, Sigma-Aldrich) was introduced into the chamber through a variable high precision leak valve after being degassed by multiple freeze–pump–thaw cycles. CO_2 (purity ≥ 99.995%, Abelló Linde) was introduced into the chamber directly from a commercial cylinder through a variable high precision leak valve. The gases were dosed into the chamber until reaching a base pressure of 5×10^{-2} mbar (CO_2:H_2O 7:1). Data were collected using SpecsLab software.

2.9. In-situ ^1H and ^{13}C solid state NMR

Analyzes were conducted in a Bruker AvanceTM 400 spectrometer equipped with a 9.4 T superconducting magnet (^1H and ^{13}C Larmor frequencies at 400.14 MHz and 100.61 MHz, respectively). For the measurements, calcined TiO_2 powder (0.1 g) was loaded in a 10 mm φ glass tube and degassed at 150 °C for 5–8 h. Samples were allowed to cool down to room temperature under vacuum, and then $^{13}CO_2$ was loaded at 1.3–2.0 bar. In water co-feeding experiments, TiO_2 powder was cooled to − 60 °C (mixture of dry ice and isopropanol) before injecting 0.1–0.2 μL of distilled water in the glass tube. Samples were irradiated under UV light (6 W lamp, $\lambda_{max} = 365$ nm) at different time intervals. Analyzes were performed using a NMR probe head with a 10 mm radiofrequency (rf) insert tuned to the ^{13}C Larmor frequency. ^{13}C NMR spectra were acquired using a single pulse excitation with solution-like NMR conditions and keeping the samples static. After this, a fraction of the sample (about 0.07 g of 0.7 g) was transferred under dry nitrogen to a 4 mm zirconia rotor, and analyzed using a standard Bruker double resonance 4 mm cross-polarization (CP)/magic angle spinning (MAS) NMR probe head. ^1H and ^{13}C MAS spectra were acquired using spinning rates of 5–6.5 kHz and a single pulse excitation with recycle delays of 5 and 3 s, respectively. The ^{13}C CP/MAS spectra were acquired with 2 ms CP contact time, a repetition rate of 3 s and high-power proton decoupling of 75 kHz. ^1H and ^{13}C chemical shifts were externally referenced to adamantane (29.5 ppm relative to tetramethylsilane, 0.0 ppm). All free-induction decays were subjected to standard Fourier transformation with 20–100 Hz line broadening and phasing. NMR spectra were evaluated using the software package XWIN NMR provided by the spectrometer manufacturer. Each spectrum was deconvoluted using Gaussian/Lorentzian fits, taking into consideration available information in the literature and our experimental observations for initial peaks assignments to carboxylated species in the region of interest. The peak areas were normalized to sample weight.

3. Results and discussion

3.1. Photocatalytic reduction of CO_2

Fig. 1c depicts the photoactivity of the TiO_2 catalyst (Fig. S1) in a gas phase photoreactor (Scheme S1) using a mixture of CO_2 and water vapor and UV illumination. CO and H_2 were obtained as main products, reaching maximum formation rates of 25.5 and 7.6 μmol g_{cat}^{-1} h^{-1}, respectively, and a photonic efficiency towards CO of 0.21% (Table S2). Besides, minor amounts of CH_3OH, CH_4 and C_2H_6 were also detected with evolution rates increasing when CO and H_2 yields decreased (Table S3). These values are comparable to other studies reported under similar conditions (Table S1), although significant differences have also been found in the literature (see Fig. 1a). To understand the dispersion in TiO_2 reactivity it is necessary to dig deeper into the mechanism that controls this reaction. In addition, $^{13}CO_2$ reduction batch reactions performed under similar reaction conditions [38] showed the production of ^{13}CO, while other products were below the detection limit of our equipment.

Activity and selectivity are governed by two main kinetic processes related to the charge dynamics of photogenerated e^-/h^+ pairs [24,25] and to the surface adsorption-desorption rates, which are intimately associated with the acid/base properties of the catalyst surface. TiO_2 presents a weakly acidic surface (PZC ≈ 6) (Fig. 2), bearing Lewis acid sites (LAS) such as Ti cations, and Brönsted acidic and basic sites (BAS and BBS) such as bridging and terminal hydroxyl groups (OH_B and OH_T, respectively)[39,40]. NH_3- and CO_2-TPD measurements (Fig. S2) confirmed that TiO_2 (PC500) mainly contains weak acid sites and intermediate basic sites, under our tested conditions, bearing an overall acidity and basicity of 0.85 and 0.37 mmol g^{-1}, respectively.

The electronic structure of TiO_2 (Fig. 2b) shows that the valence band (VB) is composed by O 2p bonding (at 7.6 eV) and non-bonding orbitals (at 5.6 eV), while the conduction band (CB) consists of Ti 3d orbitals. Upon bandgap (Eg = 3.2 eV) excitation, photogenerated electrons are transferred from non-bonding O 2p to Ti 3d orbitals [41,42], leading to the formation of less acidic LAS Ti^{3+} states (Fig. 2a bottom) and charge deficient oxygen ions (trapped holes $O^{\delta-}$), as confirmed by

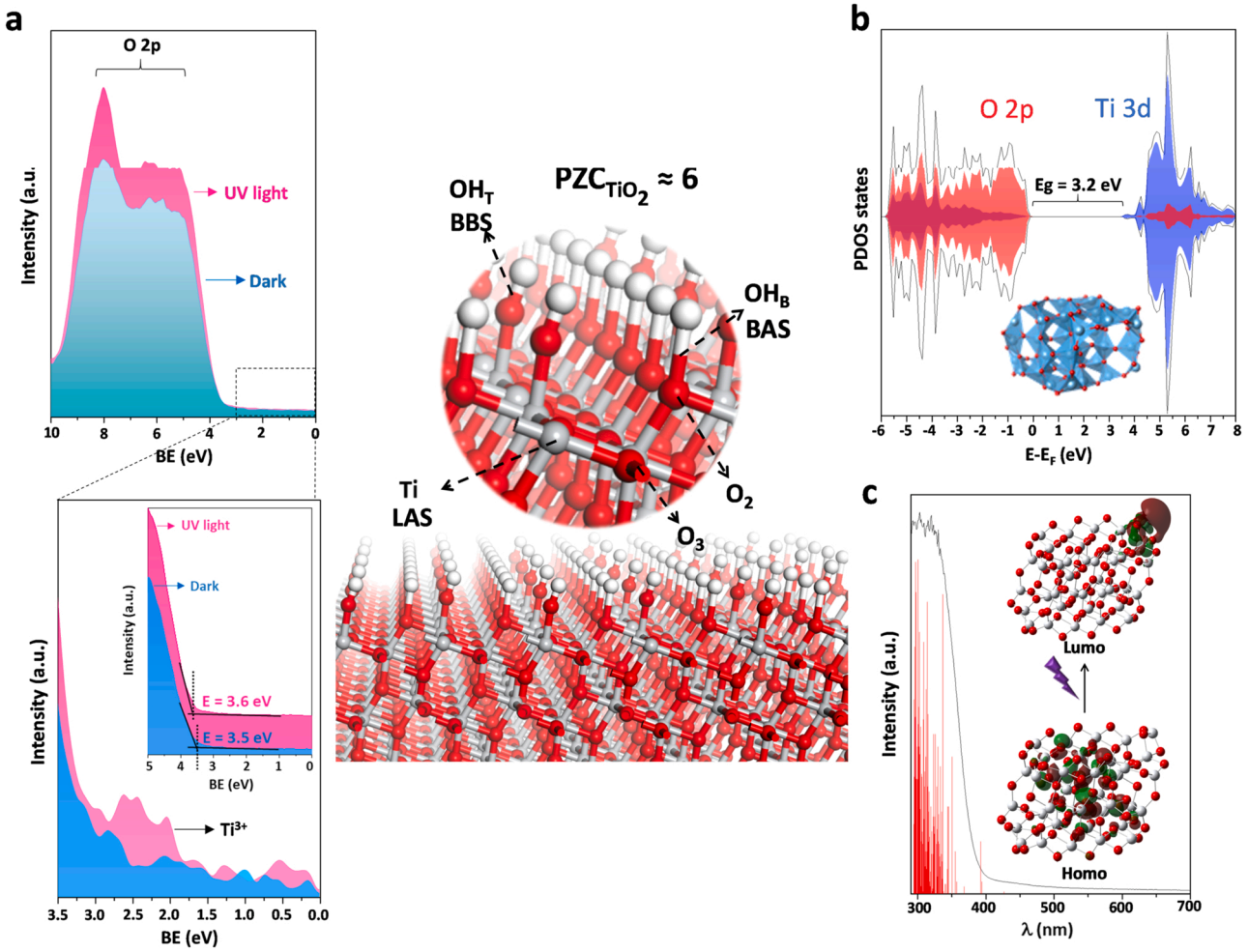

Fig. 2. Schematics of the TiO_2 anatase surface on the (101) facet, depicting Lewis acid sites (LAS) such as Ti sites, and Brönsted acid and basic sites (BAS and BBS) such as bridging and terminal hydroxyl groups (OH_B and OH_T, respectively). O_2 and O_3 stands for bicoordinated and tricoordinated oxygen atoms, respectively (center); (a) XPS valence band (VB) spectra (top) and magnification of the VB (bottom), both recorded in the dark and under UV illumination (365 nm); (b) Total density of states (DOS, black) and atom-projected density of states (PDOS) for O 2p (red) and Ti 3d (blue); (c) Comparison of the DRS UV–vis spectra of TiO_2 and the UV lamps spectra (red bars) used for the photocatalytic studies. Inset depicts the HOMO-LUMO (Highest Occupied- and Lowest Unoccupied-Molecular Orbital, respectively) electronic transition in TiO_2 upon bandgap excitation. Atom colors: light gray for Ti, red for O and white for H.

TD-DFT calculations (Fig. 2c). TD-DFT calculations show that this optical electronic transition implies a charge transfer from the Highest Occupied Molecular Orbital (HOMO) principally constituted by O2p, to the Lowest Unoccupied Molecular Orbital (LUMO), mainly formed by Ti 3d contributions (Fig. 2c).

In addition, the evaluation of CO_2 photoreduction cannot discard other additional carbon source coming from impurities initially adsorbed on the catalyst, which may contribute to the production of CO through carbon gasification or a reverse Boudouard reaction [18]. To evaluate this contribution, prior to photocatalytic experiments, we confirmed by elemental analysis and thermogravimetric studies (Fig. S3) that the calcined TiO_2 surface was relatively free of organic residues (< 0.1% wt. carbon content). XPS C 1 s spectra (Fig. S4) revealed that remaining C-residues are mainly constituted by aliphatic carbon (C-C, 284.1 eV), carbonates (CO_3^{2-}, 288.1 eV), bicarbonates (HCO_3^-, 289.2 eV), and other carbon species with methoxy (C-O, 285.5 eV) and carboxylate/carbonyl groups (COO^-/C═O, 286.8 eV) [43–45], which probably originate from exposure to the environment. C-O and COO^- species are reactive under UV illumination (Fig. S4 and Table S4), while carbonate species remain stable on the surface and only decompose partially at high temperatures (> 900 °C) (Fig. S3b). These photochemical processes are fast and occur during the first stages of the reaction. On the other hand, water oxidation competes with C-decomposition over the surface oxidation sites. UV irradiation causes a loss of physisorbed water and a slight increase in surface OH groups (Fig. S5 and Table S5), which is associated with the photoinduced superhydrophilicity of TiO_2 [21,46,47] that may contribute to the formation of bicarbonate and peroxocarbonate species.

To ascertain the influence of reactants and surface carbon species on the photocatalytic performance of TiO_2, and considering the aforementioned scenario, we carried out a series of photocatalytic experiments under different reaction atmospheres: (1) humid argon, (2) argon, and (3) dry CO_2, which led to different product distributions (see Fig. 3 and Fig. S6a). Analogously to CO_2+H_2O experiments, tests under humid argon predominantly yielded CO and H_2 (Fig. 3a), although productions decreased by half (Table S3). Photocatalytic experiments under humid argon have been proposed in the literature as a possible pretreatment to avoid the effect of C-residues[12]. On this basis, we performed two consecutive experiments: (i) humid argon and (ii) subsequent CO_2+H_2O feeding (Fig. S6b), and we did not observe the recovering of the initial production. In-situ DRIFTS experiments (Fig. S6c) showed that the production under humid argon mainly comes from inherent surface carbon species (both organics and carbonates), which corroborates XPS findings (Fig. S4). On the other hand, photocatalytic tests conducted under dry argon and CO_2 atmospheres mainly yielded CH_4 with minor amounts of CO (Fig. 3b, c). It is worth noting that CH_4 productions

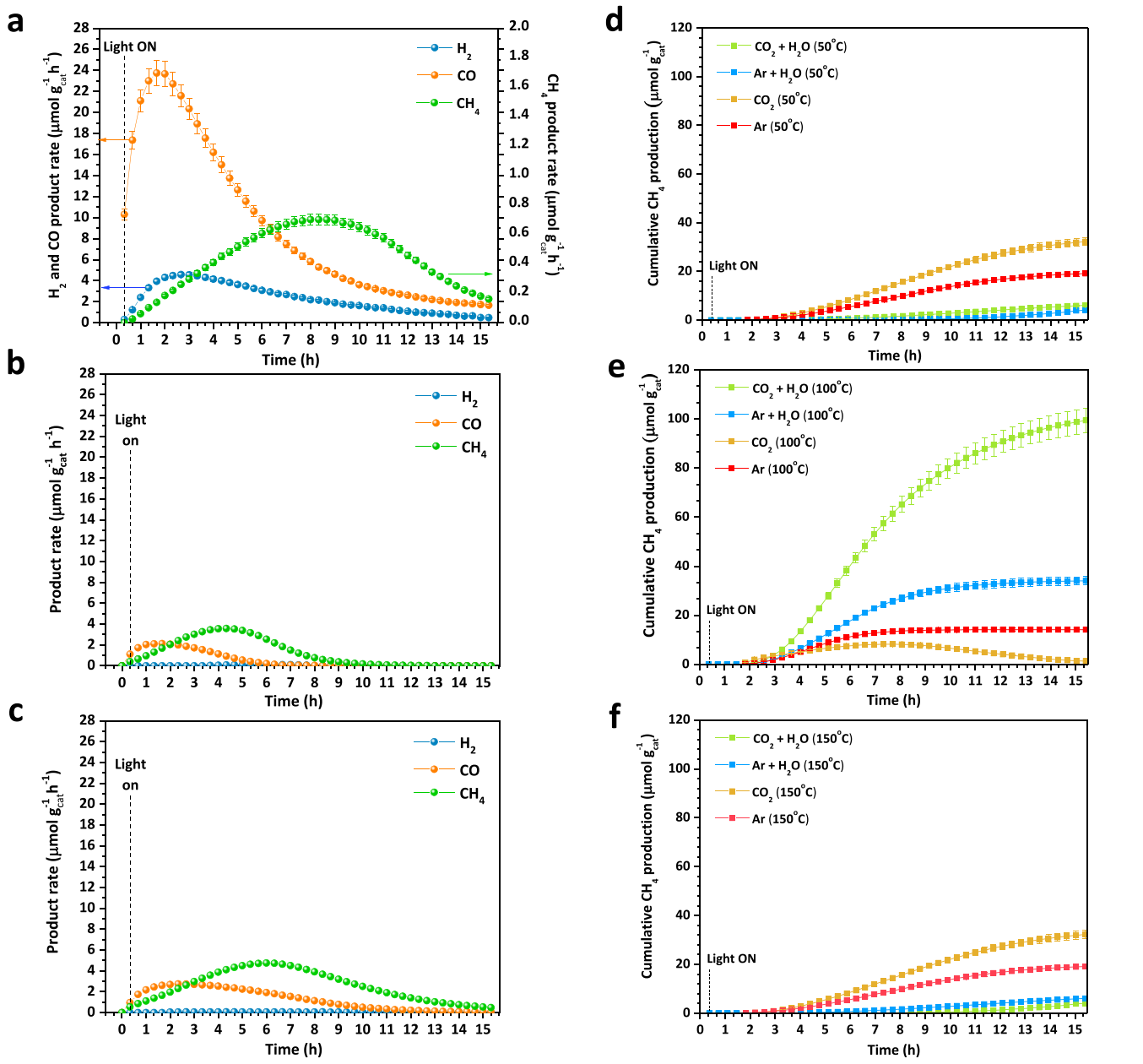

Fig. 3. (a-c) Product evolution on TiO_2 at 50 °C under UV illumination (365 nm) and the following reaction atmospheres: Ar-H_2O (a), dry Ar (b), and dry CO_2 (c); (d-f) Cumulative methane production under UV illumination (365 nm) at 50 (d), 100 (e) and 150 °C (f) under different reaction atmospheres (error bars ± 5%).

surpassed that obtained in the CO_2+H_2O experiment, being 3 and 7-times higher under dry Ar and CO_2 atmosphere, respectively (Table S3). This increase in CH_4 production is related to the absence of water adsorption competition, as well as the mediation of surface hydroxyl groups and H atoms from dissociated water [18,21] from adsorbed ambient moisture. The formation of carbon-containing products in the absence of CO_2 co-feeding is associated with the photoinduced decomposition of adsorbed carbonate- and bicarbonate-like species or other carbon residues [18], which cannot be removed by calcination due to their high decomposing temperature (see Fig. S3b).

With the aim of drawing a complete picture of the reaction mechanism, we further studied the potential back-reactions of intermediates and products. To do so, TiO_2 reactivity was evaluated in a hydrocarbon standard gas mixture (containing 100 ppm of hydrogen, carbon monoxide, methane, ethane, ethylene, propane and butane) under dry and humid Ar atmosphere (Fig. S7). Photocatalytic experiments mainly conduced to the formation of CH_4 and CO, respectively. These results show that surface carbon species, OH groups and adsorbed water contribute to the evolution of CO and hydrocarbons (e.g. CH_4), as later confirmed by in-situ DRIFT experiments. The photocatalytic tests under low humidity conditions and reaction temperatures higher than 100 °C (Fig. 3e-f) showed an unusually high selectivity to CH_4, despite most of the adsorbed water layers are removed. This suggests that the presence of water layers play a critical role in the reaction mechanism, particularly promoting CO formation.

A combination of in-situ surface studies was employed to get a deeper understanding of the influence of reactants and intermediates on CO_2 photoreduction. In-situ DRIFTS has already established itself as a powerful tool to study the reaction intermediates, and therefore it has been extensively reported in the literature (see Table S6). However, from our point of view, these studies can only illustrate the complex surface chemistry of the process, rather than provide conclusive evidence of the reaction mechanism. Fig. 4a compiles a thorough literature review of the vibrations of the main intermediates species detected in

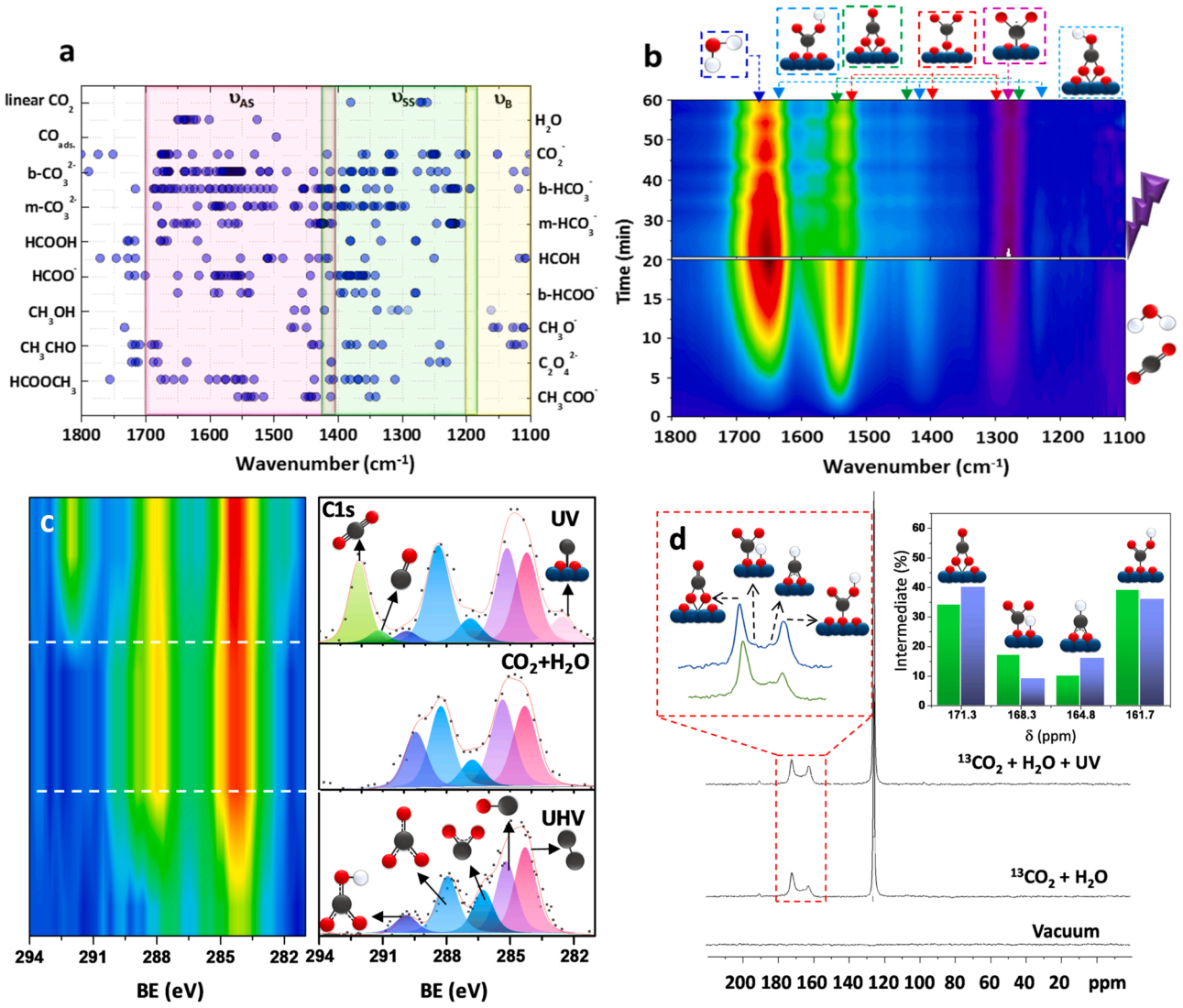

Fig. 4. (a) Representation of IR band assignments (blue dots) and their corresponding stretching (υ_{AS}, υ_{SS}) and bending (υ_B) vibrations of water and the most common surface carbon species on TiO_2 (see Table S6); (b) In-situ DRIFTS of TiO_2 under CO_2+H_2O atmosphere in the dark (bottom) and under UV illumination (top); (c) In-situ NAP-XPS C 1s region recorded for TiO_2 under ultra-high vacuum (UHV); after dosing CO_2 and H_2O at P = $4.375 \cdot 10^{-2}$ and $6.250 \cdot 10^{-3}$ mbar, respectively; and under UV illumination (365 nm); (d) ^{13}C MAS NMR spectra of TiO_2 after the following treatment: 5 h at 150 °C under vacuum; exposed to $^{13}CO_2$ and moist; and exposed to $^{13}CO_2$, moist and UV irradiation (365 nm) during 6 h. The expanded spectral regions show the peak assignment to various carboxylated species, and the inset graph illustrates the corresponding individual peak areas calculated by deconvolution of the NMR spectra and the total signal normalized to sample weight. Sequence of colors in the contour plots from red to blue correspond to high to low intensity, respectively.

CO_2 photoreduction with TiO_2. The evident overlapping of signals, derived from the high dispersion of reported data, complicates an unambiguous identification of surface species. The most plausible interpretation of our results (Fig. 4b) suggests that CO_2 and H_2O dosing promotes the formation of carbonate, bicarbonate and CO_2^- species (ca. 1250–1620 cm^{-1}) in different adsorption modes. Under UV illumination, there is a partial loss of the surface water layer that is accompanied by a decrease in HCO_3^- species (ca. 1210–1230 cm^{-1}), and a parallel increase in b-CO_3^{2-} and CO_2^- species (ca. 1275 cm^{-1}). To confirm DRIFTS observations, we carried out further in-situ spectroscopic studies to undoubtedly identify the evolution of carbonate-like species and the formation of reaction intermediates.

Raman studies under UV illumination corroborated the significant formation of b-CO_3^{2-} and m-CO_3^{2-} from HCO_3^- species (Fig. S8a). Irradiation also conduced to the formation of formates (ca. 1371 and 1565 cm^{-1}) and interestingly led to the appearance of peroxocarbonates and superoxo-like species (ca. 988 and 1130 cm^{-1}, respectively). The formation of peroxocarbonates may follow two pathways: (i) perhydration (reaction of CO_2 with H_2O_2), followed by deprotonation to form HCO_4^-; and/or (ii) direct reaction of CO_2 with a hydroperoxide ion (HO_2^-). The latter pathway dominates at mild basic pH due to the higher contribution of the conjugate base HO_2^-, while more acidic pH increases the dehydration of bicarbonates toward CO_2 to form HCO_4^- [48].

Near Ambient Pressure XPS (NAP-XPS) in the C1s region also unveiled an increase in carbonate/bicarbonate species, especially bicarbonates, after exposure to CO_2 and H_2O atmosphere (Fig. 4c and Table S7) [43,44]. An increase in C═O/COO^- groups (ca. 286.2 eV) was also observed, most probably corresponding to carboxylates of formate species. On the contrary, the signal of C-O groups (ca. 285.3 eV) increased, in good agreement with the appearance of a new component in O 1 s spectra (Fig. S9) associated to carbon-oxygen groups (ca. 532.3 eV), such as methoxy species. This suggests that, even in dark conditions, the surface acidity of TiO_2 (protons over the surface) favors the conversion of formate to methoxy species.

Under UV illumination, C 1s spectra (Fig. 4c) showed an overall depletion of bicarbonates, carbonyl/carboxylates and methoxy groups,

in good agreement with a decrease in the C-O signal in O 1s spectra (see Tables S7 - S8). In addition, two new components appeared in the C 1s spectra attributed to CO_2^- and/or gas-phase CO (291.1 eV), and photo-desorbed gas-phase CO_2 [49,50] (292.1 eV) (Fig. 4c). The O 1s spectra also revealed a new peak at ca. 536.1 eV that can be assigned to the formation of both gas phase CO and/or CH_3OH [43,50,51] (Fig. S9). It should be noted that CH_3OH could not be identified in C 1 s spectra due to an overlapping with the carbonate region (ca. 288–290 eV) [43,51].

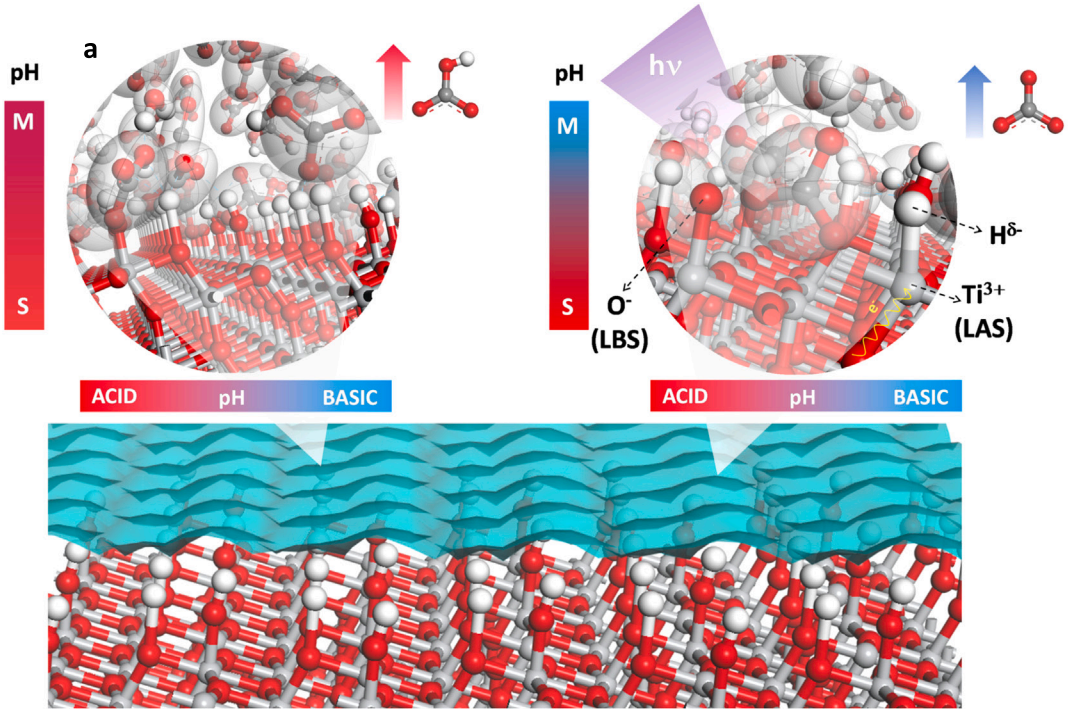

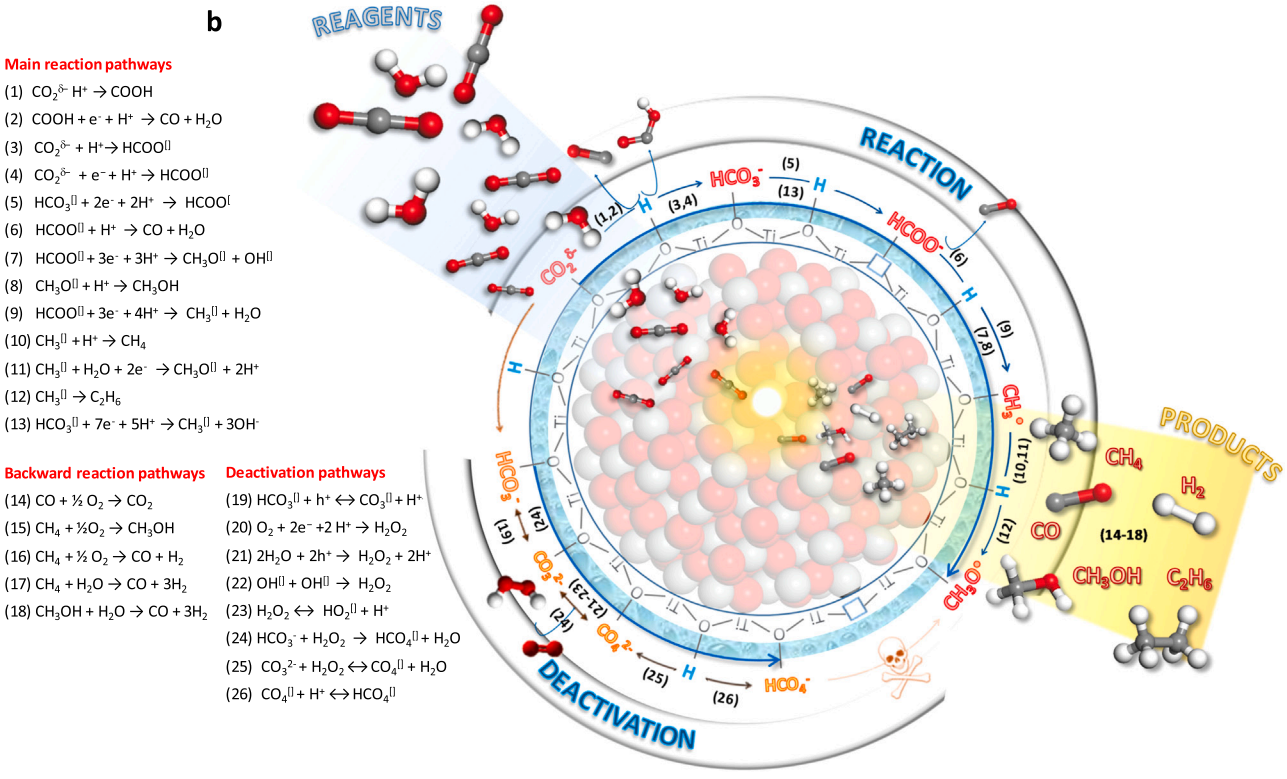

Fig. 5. (a) Influence of reaction conditions on the evolution of the acid/basic TiO_2 surface chemistry, under dark (left) and UV illumination (right) conditions. Horizontal bars display the pH color range from acid (red) to basic (blue), while vertical color bars indicate the changes in the pH on both TiO_2 surface (S) and reactive medium (M). LAS and LBS stands for Lewis acid and basic sites, respectively; (b) Main, backward and deactivation reactions pathways for CO_2 photoreduction over TiO_2; [] refers to adsorbed molecules. Atom colors: light gray (Ti), red (O), dark gray (C) and white (H).(For interpretation of the references to colour in this figure legend, the reader is referred to the web version of this article.)

Moreover, a decrease in OH groups was observed along the reaction in O 1s spectra (Table S8), suggesting the contribution of these species in the photoredox process. This observation agrees well with the depletion of hydroxyl groups and adsorbed H_2O under illumination, observed in ^1H MAS NMR spectra (Fig. S10) and DRIFTS (Fig. S11) under reaction conditions.

In-situ ^{13}C MAS NMR measurements, upon H_2O and CO_2 dosage (Fig. 4d), showed a narrow signal characteristic of physisorbed $^{13}CO_2$ at 125 ppm, together with two broad features at ca. 160 and 170 ppm. The presence of wide bands is representative of disordered water in different chemical environments [52]. A more detailed study of this region led to the identification of four resonances, which can be tentatively assigned to: (i) bidentate carbonates (171.3 ppm), (ii) carbonates (168.3 ppm) interacting with OH^- or H_2O via H-bridge interactions (i.e. hydroxycarbonates), (iii) formates (164.8 ppm) and (iv) bicarbonates (161.7 ppm) (Table S9). $^{13}CP/MAS$ NMR (Cross Polarization/Magic Angle Spinning Nuclear Magnetic Resonance) spectra, which show carbon atoms with protons in their vicinity, allowed to distinguish bicarbonates, formates and hydroxycarbonates (Fig. S12a). The new contribution at 171.8 ppm can be associated with carboxylates close to OH surface groups.

In addition, $^{13}CO_2$ static NMR spectra revealed a resonance at 49 ppm attributed to methoxy groups (Fig. S12b), which increased upon illumination. These findings agree with NAP-XPS observations and confirm the catalytic conversion of formates to methoxy species via by an acid mechanism over TiO_2, even in the dark [53]. These observations are consistent with ^1H MAS NMR spectra (Fig. S10), which showed a small contribution at ca. 3–5 ppm region that could be tentatively assigned to the formation of CH_3 or CH_3O^- intermediates under prolonged UV illumination. We note that the broadening of this signal may also suggest the presence of peroxide species (see Table S9). ^{13}C CP/MAS NMR, NAP-XPS and Raman studies (Fig. S13 and Fig. S8) further revealed that a prolonged light exposure leads to the stabilization of an overlayer of unreactive carbonates and peroxocarbonates that contributes to the blockage of TiO_2 active sites, leading to its deactivation.

3.2. Proposed pathway of CO_2 reduction

Based on our observations from in-situ surface studies and photocatalytic experiments, we propose a CO_2 photoreduction mechanism based on multiple parallel reactions with consecutive steps, which strongly depend on the experimental conditions and the dynamic changes occurring on the surface along the reaction (Fig. 5).

Initially, calcined TiO_2 surface contains traces of unspecific carbon species (principally organic residues, carbonate-like species and methoxy/carboxylate groups), coming from the synthesis or the adsorption from air. After CO_2:H_2O dosage, the surface is covered by a thin layer of water in which CO_2 is partially solvated/dissolved (0.2 – 1% as carbonic acid), [21] causing a surface acidification below the point of zero charge of TiO_2 ($pH_{PZC} \sim 6$). This promotes the formation of carbonates (CO_3^{2-}) with different coordination geometries on titanium sites (Fig. S14). Surface hydroxyl groups (OH^-) interact with reagents and intermediates in the reaction medium (see video S1 in Supplementary Material). Thus, the interaction of carbonic acid with surface OH^- leads to dehydration and binding of bicarbonates (HCO_3^-) [21,48].

Undercoordinated titanium sites (Lewis acid sites) and vicinal hydroxyl groups (Lewis basic sites) can likely form metastable surface frustrated Lewis pairs (SFLP), which enhance the formation of adsorbed/activated CO_2 ($CO_2^{\delta-}$) or carboxylates [14–16,54,55]. These species are preferentially formed in the absence of water. It is also important to highlight that the nature and concentration of surface carbon species vary depending on the reaction conditions, such as temperature and water content, the latter also influencing the pH of both the reaction medium and the catalyst surface.

UV illumination promotes a charge transfer from oxygen to titanium atoms, leading to titanium reduction ($O^{\delta-} \rightarrow Ti^{3+}$) and the formation of surface oxygen vacancies (O_V) [46,56–58], which are the main active sites for redox reactions. Besides, illumination induces changes on the acidity of the hydroxyl groups (Fig. 5a), stimulating the protonation of Ti−O−Ti sites (acidic OH groups) rather than promoting the direct bonding of OH^- to 5-coordinated Ti ions (basic Ti-OH species) [59]. The photogenerated less acidic Lewis sites (Ti^{3+}) favor the conversion of monodentate carbonates (m-CO_3^{2-}) into bidentate-like carbonates through oxygen vacancies filling [60]. This reaction is also favored by a partial water desorption (Fig. S6 and Fig. S11).

In addition, in the first reaction steps $CO_2^{\delta-}$ is protonated to carboxylic acid (COOH), which can be reductively dissociated in acidic media to CO and H_2O (Fig. 5, Eq. 1, 2 respectively). In contrast, the formation of formates ($HCOO^-$), can be directly promoted by reaction of $CO_2^{\delta-}$ with neighboring Ti–H [61] (acidic mechanism) or by a proton-coupled electron transfer (PCET) process (equations 3, 4 respectively). Formates can also be formed by a direct two-electron reduction of adsorbed bicarbonate HCO_3^- (equation 5). Then, formates can follow different and not mutually exclusive pathways: a) decomposition in acidic media to produce CO (equation 6), promoted by a weaker binding on SFLP [21,62]; b) reduction to methoxy (CH_3O) intermediate to produce methanol (equations 7,8); c) hydrogenation to methyl (CH_3) intermediates (equation 9) and subsequent formation of methanol, methane or C^{2+} products (equations 10–12). On the order hand, adsorbed bicarbonates can be reduced via PCET to methyl intermediates (equation 13) and then to the subsequent products (equations 8, 10–12).

In our study, we have confirmed that reaction pathways strongly depend on the interaction between condensed water and the catalyst surface. Under low surface moisture conditions (Fig. 3b,c) or high temperature (Fig. 3e,f), formate species preferentially dissociate on O_V to methyl radicals [22], leading to the formation of CH_4 and further coupling to form other hydrocarbons (mainly C_2H_6) [23,63] (Fig. 5, equation 12). On the contrary, higher amounts of water (Fig. 3a) leads to the formation of a condensed water layer over the catalyst surface. As previously commented, the acidic/basic properties of the solvent/catalyst interface change along the reaction, thus modifying the reaction mechanism. Namely, favoring the direct dissociation of formate to CO, or in minor extent to methoxy species, due to a competitive adsorption of water on O_V [21,55].

Furthermore, our experiments (Fig. S7, Fig. S15-16) have shown that other competitive backward reactions can occur in the presence of O_2: a) oxidation of CO to CO_2 (Fig. 5, equation 14); b) partial oxidation of CH_4 to methanol or syngas (equations 15, 16); or in the presence of water: c) photoreforming of CH_4 or CH_3OH towards CO and H_2 [23,64] (Fig. 5, equations 17, 18). Therefore, water content influences both the production and selectivity of TiO_2, suggesting that CO_2 adsorption may be a rate limiting step.

Stability studies show that reactions leading to catalyst deactivation are promoted by both photoinduced charges and acid/base properties. Thus, bicarbonates can act as hole scavengers [21] leading to the formation of carbonates that will be strongly adsorbed on the TiO_2 surface (Fig. 5, equation 19). In addition, ^{13}C CP/MAS NMR measurements (Fig. S13) unveiled the formation of adsorbed peroxocarbonates by a slight broadening of the bicarbonate resonance (ca. 159.2 ppm), as previously revealed in Raman studies (Fig. S8). These species are formed in a series of consecutive steps. First, peroxo species (H_2O_2, HO_2^-) are formed by the reaction of water or O_2 with holes or electrons, respectively [11,65,66] (Fig. 5, equations 20–23). Peroxo species induce a light yellowish color on the TiO_2 surface (Fig. S8c), which disappears under UV illumination by decomposition to $OH^\bullet$ radicals with surface-trapped electrons (Ti^{3+}). The oxygen consumption in the formation of peroxo-species and the partial oxidation of products explains the lack of net O_2 production during CO_2 photoreduction (Fig. S15-S16).

This study evidences that prolonged UV irradiation leads to the stabilization of surface carbonate, peroxo- and peroxocarbonate species that, together with the slow desorption of products, contribute to the

blocking of TiO_2 active sites and its deactivation. The deactivation of TiO_2 centers seems to occur in the first stages of the reaction and is mostly irreversible, constituting the main drawback of this catalyst. We explored two regeneration strategies: i) Thermal treatment at temperatures higher than 900 °C for the removal of surface carbonates (see Fig. S3b), which leads to small activity recoveries (< 1%), an unavoidable loss of surface area and changes in the structural and chemical properties of TiO_2; and ii) Acid washing of the catalyst surface after reaction with a mild acid solution. This method is effective to dissolve the adsorbed carbonate species and to acidify the surface, which result in a partial TiO_2 regeneration (ca. 23% for CO evolution, see Fig. S17).

4. Conclusions

Based on the results and insights gained from this work, we provided clear evidences about the catalytic pathways influencing the activity, selectivity and stability of TiO_2 in CO_2 photoreduction, which are mainly governed by PCET processes. In addition, the presence of acidic and basic sites leads to the formation of a significant number of intermediates and products (such as formates and methanol), which are also detected under dark conditions. UV illumination induces relevant changes not only in the redox properties of the TiO_2 active sites, but also in the acid/base character of the surface and the medium, which plays a key role in the selectivity and deactivation pathways.

In addition, our results call into question some key issues that were unclear up to date, and which are highly relevant to deactivation pathways. Thus, TiO_2 deactivation is mainly initiated by the formation of carbonates and peroxo- species favored by the presence of oxygen, which also participates in the partial oxidation of products, thus explaining the lack of net O_2 production. Lastly, TiO_2 activity can be partially recovered by a post-reaction washing treatment with a mild acid solution.

These findings enlighten the main shadows remaining unclear on the CO_2 photoreduction mechanism, and at the same time, shed light on the factors controlling the activity and stability. In addition, this work lays the foundation for the rational design of efficient photocatalysts, which may be of great interest for a multitude of potential applications such as water splitting, biomass photoreforming, ammonia production and other light-driven catalytic reactions for renewable energy applications.

CRediT authorship contribution statement

LC: Methodology, Investigation, Writing – original draft, Writing – review & editing, Visualization. **PR**: Investigation, Writing – review & editing. **JF:** Investigation, Writing – review & editing. **FF**: Investigation, Writing – review & editing. **LG**: Investigation, Writing – review & editing. **VPD**: Investigation, Writing – review & editing. **C.E**: Investigation, Writing – review & editing. **MDHA**: Writing – review & editing. **JMC:** Methodology, Writing – review & editing. **DS**: Methodology, Writing – review & editing. **VAPO:** Conceptualization, Methodology, Writing – review & editing, Supervision.

Declaration of Competing Interest

TThere are no conflicts of interest to declare.

Acknowledgements

This work was supported by MINECO (PID2019-106315RB-I00). Authors also wish to thank Comunidad de Madrid and European Structural Funds for their financial support for FotoArt-CM project (S2018/NMT-4367) and Fundación Ramón Areces. The authors also thank ALBA Cells Synchrotron (Barcelona, Spain) and CSUC supercomputing center for funded access to their facilities.

Author contributions

All authors have given approval to the final version of the manuscript.

Appendix A. Supporting information

Supplementary data associated with this article can be found in the online version at doi:10.1016/j.apcatb.2021.120931.

References

[1] M. Shen, L. Zhang, J. Shi, Defect engineering of photocatalysts towards elevated CO_2 reduction performance, ChemSusChem 14 (2021) 1–21, https://doi.org/10.1002/cssc.202100677.
[2] R.C. Armstrong, C. Wolfram, K.P. De Jong, R. Gross, N.S. Lewis, B. Boardman, A. J. Ragauskas, K. Ehrhardt-Martinez, G. Crabtree, M.V. Ramana, The frontiers of energy, Nat. Energy 1 (2016) 1–8, https://doi.org/10.1038/nenergy.2015.20.
[3] S. Chu, A. Majumdar, Opportunities and challenges for a sustainable energy future, Nature 488 (2012) 294–303.
[4] M. Tasbihi, F. Fresno, I. Álvarez-Prada, A. Acharjya, A. Thomas, L. Escriche, N. Romero, X. Sala, V.A. de la Peña O'Shea, J. García-Antón, A molecular approach to the synthesis of platinum-decorated mesoporous graphitic carbon nitride as selective CO_2 reduction photocatalyst, J. CO_2 Util. 50 (2021) 101574–101583, https://doi.org/10.1016/j.jcou.2021.101574.
[5] W. Zhang, A.R. Mohamed, W.J. Ong, Z-scheme photocatalytic systems for carbon dioxide reduction: where are we now? Angew. Chem. - Int. Ed. 59 (2020) 22894–22915, https://doi.org/10.1002/anie.201914925.
[6] R.E. Blankenship, D.M. Tiede, J. Barber, G.W. Brudvig, G. Fleming, M. Ghirardi, M. R. Gunner, W. Junge, D.M. Kramer, A. Melis, T.A. Moore, C.C. Moser, D.G. Nocera, A.J. Nozik, D.R. Ort, W.W. Parson, R.C. Prince, R.T. Sayre, Comparing photosynthetic and photovoltaic efficiencies and recognizing the potential for improvement, Science 332 (2011) 805–809, https://doi.org/10.1126/science.1200165.
[7] J. Su, L. Vayssieres, A place in the sun for artificial photosynthesis? ACS Energy Lett. 1 (2016) 121–135, https://doi.org/10.1021/acsenergylett.6b00059.
[8] V.A. de la Peña O'Shea, D.P. Serrano, J.M. Coronado, Current Challenges of CO_2 Photocatalytic Reduction Over Semiconductors Using Sunlight, Springer, London, 2015.
[9] M. Liras, M. Barawi, V.A. De La Peña O'Shea, Hybrid materials based on conjugated polymers and inorganic semiconductors as photocatalysts: From environmental to energy applications, Chem. Soc. Rev. 48 (2019) 5454–5487, https://doi.org/10.1039/c9cs00377k.
[10] J.K. Stolarczyk, S. Bhattacharyya, L. Polavarapu, J. Feldmann, Challenges and prospects in solar water splitting and CO_2 reduction with inorganic and hybrid nanostructures, ACS Catal. 8 (2018) 3602–3635, https://doi.org/10.1021/acscatal.8b00791.
[11] F. Fresno, I.J. Villar-García, L. Collado, E. Alfonso-González, P. Reñones, M. Barawi, V.A. de la Peña O'Shea, Mechanistic view of the main current issues in photocatalytic CO_2 reduction, J. Phys. Chem. Lett. 9 (2018) 7192–7204, https://doi.org/10.1021/acs.jpclett.8b02336.
[12] L. Collado, T. Naranjo, M. Gomez-Mendoza, C.G. López-Calixto, F.E. Oropeza, M. Liras, et al., Conjugated porous polymers based on BODIPY and BOPHY dyes in hybrid heterojunctions for artificial photosynthesis, Adv. Funct. Mater. (2021) 2105384–2105396, https://doi.org/10.1002/adfm.202105384.
[13] M. Barawi, L. Collado, M. Gomez-Mendoza, F.E. Oropeza, M. Liras, V.A. de la Peña O'Shea, Conjugated porous polymers: ground-breaking materials for solar energy conversion, Adv. Energy Mater. 2101530 (2021) 1–31, https://doi.org/10.1002/aenm.202101530.
[14] K.K. Ghuman, L.B. Hoch, P. Szymanski, J.Y.Y. Loh, N.P. Kherani, M.A. El-Sayed, G. A. Ozin, C.V. Singh, Photoexcited surface frustrated Lewis Pairs for heterogeneous photocatalytic CO_2 reduction, J. Am. Chem. Soc. 138 (2016) 1206–1214, https://doi.org/10.1021/jacs.5b10179.
[15] M. Ghoussoub, S. Yadav, K.K. Ghuman, G.A. Ozin, C.V. Singh, Metadynamics-biased ab initio molecular dynamics study of heterogeneous CO_2 reduction via surface frustrated Lewis Pairs, ACS Catal. 6 (2016) 7109–7117.
[16] Y. Dong, K.K. Ghuman, R. Popescu, P.N. Duchesne, W. Zhou, J.Y.Y. Loh, A.A. Jelle, J. Jia, D. Wang, X. Mu, C. Kübel, L. Wang, L. He, M. Ghoussoub, Q. Wang, T. E. Wood, L.M. Reyes, P. Zhang, N.P. Kherani, C.V. Singh, G.A. Ozin, Tailoring surface frustrated Lewis Pairs of $In_2O_{3-x}(OH)_y$ for gas-phase heterogeneous photocatalytic reduction of CO_2 by isomorphous substitution of In^{3+} with Bi^{3+}, Adv. Sci. 5 (2018) 1700732–1700743, https://doi.org/10.1002/advs.201700732.
[17] A. Pougin, M. Dilla, J. Strunk, Identification and exclusion of intermediates of photocatalytic CO_2 reduction on TiO_2 under conditions of highest purity, Phys. Chem. Chem. Phys. 18 (2016) 10809–10817, https://doi.org/10.1039/c5cp07148h.
[18] C.-C. Yang, Y.-H. Yu, B. van der Linden, J.C.S. Wu, G. Mul, Artificial photosynthesis over crystalline TiO_2-based catalysts: fact or fiction? J. Am. Chem. Soc. 132 (2010) https://doi.org/10.1021/ja101318k, 8398–406.
[19] Art Leaf Database - CO_2 valorization by Artificial Photosynthesis. Available at: ⟨http://www.artleafs.eu⟩, (n.d.).

[20] S.E. Braslavsky, A.M. Braun, A.E. Cassano, A.V. Emeline, M.I. Litter, L. Palmisano, V.N. Parmon, N. Serpone, Glossary of terms used in photocatalysis and radiation catalysis (IUPAC Recommendations 2011), Pure Appl. Chem. 83 (2011) 931–1014, https://doi.org/10.1351/gold-book.

[21] N.M. Dimitrijevic, B.K. Vijayan, O.G. Poluektov, T. Rajh, K. Gray, H. He, et al., Role of water and carbonates in photocatalytic transformation of CO_2 to CH_4 on titania, J. Am. Chem. Soc. 133 (2011) 3964–3971, https://doi.org/10.1021/ja108791u.

[22] J.Y. Liu, X.Q. Gong, A.N. Alexandrova, Mechanism of CO_2 photocatalytic reduction to methane and methanol on defected anatase TiO_2 (101): a density functional theory study, J. Phys. Chem. C 123 (2019) 3505–3511, https://doi.org/10.1021/acs.jpcc.8b09539.

[23] L. Liu, H. Zhao, J.M. Andino, Y. Li, Photocatalytic CO_2 reduction with H_2O on TiO_2 nanocrystals: comparison of anatase, rutile, and brookite polymorphs and exploration of surface chemistry, ACS Catal. 2 (2012) 1817–1828.

[24] L. Collado, A. Reynal, F. Fresno, M. Barawi, C. Escudero, V. Perez-dieste, J. M. Coronado, D.P. Serrano, J.R. Durrant, V.A. de la Peña O'Shea, Unravelling the effect of charge dynamics at the plasmonic metal/semiconductor interface for CO_2 photoreduction, Nat. Commun. 9 (2018) 1–10, https://doi.org/10.1038/s41467-018-07397-2. Artic. Number 4986.

[25] L. Collado, A. Reynal, J.M. Coronado, D.P. Serrano, J.R. Durrant, V.A. de la Peña O'Shea, Effect of Au surface plasmon nanoparticles on the selective CO_2 photoreduction to CH_4, Appl. Catal. B Environ. 178 (2015) 177–185, https://doi.org/10.1016/j.apcatb.2014.09.032.

[26] G. Li, S. Ciston, Z.V. Saponic, L. Chen, N.M. Dimitrijevic, T. Rajh, K.A. Gray, Synthesizing mixed-phase TiO_2 nanocomposites using a hydrothermal method for photo-oxidation and photoreduction applications, J. Catal. 253 (2008) 105–110, https://doi.org/10.1016/j.jcat.2007.10.014.

[27] O. Lamiel-Garcia, K.C. Ko, J.Y. Lee, S.T. Bromley, F. Illas, When anatase nanoparticles become bulklike: properties of realistic TiO_2 nanoparticles in the 1–6 nm size range from all electron relativistic density functional theory based calculations, J. Chem. Theory Comput. 13 (2017) 1785–1793.

[28] G. Kresse, J. Furthmüller, Efficiency of ab-initio total energy calculations for metals and semiconductors using a plane-wave basis set, Comput. Mater. Sci. 6 (1996) 15–50, https://doi.org/10.1016/0927-0256(96)00008-0.

[29] G. Kresse, J. Hafner, Ab initio molecular dynamics for liquid metals, Phys. Rev. B 47 (1993) 558–561.

[30] J.P. Perdew, K. Burke, M. Ernzerhof, Generalized gradient approximation made simple, Phys. Rev. Lett. 77 (1996) 3865–3868.

[31] J. Heyd, G.E. Scusseria, M. Ernzerhof, Hybrid functionals based on a screened Coulomb potential, J. Chem. Phys. 118 (2003) 8207–8215.

[32] F. Furche, R. Ahlrichs, Adiabatic time-dependent density functional methods for excited state properties, J. Chem. Phys. 117 (2002) 7433–7447.

[33] G. Scalmani, M.J. Frisch, B. Mennucci, J. Tomasi, R. Cammi, V. Barone, Geometries and properties of excited states in the gas phase and in solution: theory and application of a time-dependent density functional theory polarizable continuum model, Chem. Phys. 094107 (2006) 1–15.

[34] M. Frisch, G. Trucks, H. Schlegel, G.E. Scuseria, M.A. Robb, J.R. Cheeseman, et al., Gaussian 09, Revision A.02, Wallingford CT, 2009.

[35] T. Yanai, D.P. Tew, N.C. Handy, A new hybrid exchange–correlation functional using the Coulomb-attenuating method (CAM-B3LYP), Chem. Phys. Lett. 393 (2004) 51–57.

[36] N. Godbout, D.R. Salahub, J. Andzelm, E. Wimmer, Optimization of Gaussian-type basis sets for local spin density functional calculations. Part I. Boron through neon, optimization technique and validation, Can. J. Chem. 70 (1992) 560–571.

[37] C. Sosa, J. Andzelm, B.C. Elkin, E. Wimmer, K.D. Dobbs, D.A. Dixon, A. Local, Density functional study of the structure and vibrational frequencies of molecular transition-metal compounds, J. Phys. Chem. 96 (1992) 6630–6636.

[38] F. Fresno, P. Reñones, E. Alfonso, C. Guillén, J.F. Trigo, J. Herrero, L. Collado, V. A. de la Peña O'Shea, Influence of surface density on the CO_2 photoreduction activity of a DC magnetron sputtered TiO_2 catalyst, Appl. Catal. B Environ. 224 (2018) 912–918, https://doi.org/10.1016/j.apcatb.2017.11.022.

[39] L. Ding, M. Li, Y. Zhao, H. Zhang, J. Shang, J. Zhong, H. Sheng, C. Chen, J. Zhao, The vital role of surface Brönsted acid/base sites for the photocatalytic formation of free·OH radicals, Appl. Catal. B Environ. 266 (2020) 118634–118642, https://doi.org/10.1016/j.apcatb.2020.118634.

[40] M.I. Zaki, M.A. Hasan, F.A. Al-sagheer, L. Pasupulety, In situ FTIR spectra of pyridine adsorbed on SiO_2–Al_2O_3, TiO_2, ZrO_2 and CeO_2: general considerations for the identification of acid sites on surfaces of finely divided metal oxides, Coll. Surf. A Physicochem. Eng. Asp. 190 (2001) 261–274.

[41] V.A. de la Peña O'Shea, M. Capel-Sanchez, G. Blanco-Brieva, J.M. Campos-Martin, J.L.G. Fierro, The usefulness of time-dependent density functional theory to describe the electronic spectra of Ti-containing catalysts, Angew. Chem. Int. Ed. 42 (2003) 5851–5854, https://doi.org/10.1002/anie.200351452.

[42] M.C. Capel-Sanchez, V.A. de la Peña O'Shea, L. Barrio, J.M. Campos-Martin, J.L. G. Fierro, TD-DFT analysis of the electronic spectra of Ti-containing catalysts, Top. Catal. 41 (2006) 27–34, https://doi.org/10.1007/s11244-006-0091-9.

[43] H. Bluhm, M. Hävecker, A. Knop-Gericke, E. Kleimenov, R. Schlögl, D. Teschner, V. I. Bukhtiyarov, D.F. Ogletree, M. Salmeron, Methanol oxidation on a copper catalyst investigated using in situ X-ray photoelectron spectroscopy, J. Phys. Chem. B 108 (2004) 14340–14347, https://doi.org/10.1021/jp040080j.

[44] M. Salmeron, R. Schlogl, Ambient pressure photoelectron spectroscopy: a new tool for surface science and nanotechnology, Surf. Sci. Rep. 63 (2008) 169–199, https://doi.org/10.1016/j.surfrep.2008.01.001.

[45] X. Deng, A. Verdaguer, T. Herranz, C. Weis, H. Bluhm, M. Salmeron, Surface chemistry of Cu in the presence of CO_2 and H_2O, Langmuir 24 (2008) 9474–9478, https://doi.org/10.1021/la8011052.

[46] J. Schneider, M. Matsuoka, M. Takeuchi, J. Zhang, Y. Horiuchi, M. Anpo, D. W. Bahnemann, Understanding TiO_2 photocatalysis: mechanisms and materials, Chem. Rev. 114 (2014) 9919–9986, https://doi.org/10.1021/cr5001892.

[47] R. Wang, K. Hashimoto, A. Fujishima, M. Chikuni, E. Kojima, A. Kitamura, M. Shimohigoshi, T. Watanabe, Light-induced amphiphilic surface, Nature 388 (1997) 431–432.

[48] E.V. Bakhmutova-Albert, H. Yao, D.E. Denevan, D.E. Richardson, Kinetics and mechanism of peroxymonocarbonate formation, Inorg. Chem. 49 (2010) 11287–11296, https://doi.org/10.1021/ic1007389.

[49] Y. Toda, H. Hirayama, N. Kuganathan, A. Torrisi, P.V. Sushko, H. Hosono, Activation and splitting of carbon dioxide on the surface of an inorganic electride material, Nat. Commun. 4 (2013) 1–8, https://doi.org/10.1038/ncomms3378.

[50] A. Sápi, G. Halasi, J. Kiss, D.G. Dobó, K.L. Juhász, V.J. Kolcsár, Z. Ferencz, G. Vári, V. Matolin, A. Erdőhelyi, Á. Kukovecz, Z. Kónya, In situ DRIFTS and NAP-XPS exploration of the complexity of CO_2 hydrogenation over size-controlled Pt nanoparticles supported on mesoporous NiO, J. Phys. Chem. C 122 (2018) 5553–5565, https://doi.org/10.1021/acs.jpcc.8b00061.

[51] D.E. Starr, E.K. Wong, D.R. Worsnop, K.R. Wilson, H. Bluhm, A combined droplet train and ambient pressure photoemission spectrometer for the investigation of liquid/vapor interfaces, Phys. Chem. Chem. Phys. 10 (2008) 3093–3098, https://doi.org/10.1039/b800717a.

[52] H. Nebel, M. Neumann, C. Mayer, M. Epple, On the structure of amorphous calcium carbonate - a detailed study by solid-state NMR spectroscopy, Inorg. Chem. 47 (2008) 7874–7879, https://doi.org/10.1021/ic8007409.

[53] K. Larmier, W.C. Liao, S. Tada, E. Lam, R. Verel, A. Bansode, A. Urakawa, A. Comas-Vives, C. Copéret, CO_2-to-Methanol hydrogenation on zirconia-supported copper nanoparticles: reaction intermediates and the role of the metal–support interface, Angew. Chem. Int. Ed. 56 (2017) 2318–2323, https://doi.org/10.1002/anie.201610166.

[54] X. Wang, L. Lu, B. Wang, Z. Xu, Z. Xin, S. Yan, et al., Frustrated Lewis Pairs accelerating CO_2 reduction on oxyhydroxide photocatalysts with surface lattice hydroxyls as a solid-state proton donor, Adv. Funct. Mater. 28 (2018) 1–9, https://doi.org/10.1002/adfm.201804191.

[55] T. Yan, L. Wang, Y. Liang, M. Makaremi, T.E. Wood, Y. Dai, B. Huang, A.A. Jelle, Y. Dong, G.A. Ozin, Polymorph selection towards photocatalytic gaseous CO_2 hydrogenation, Nat. Commun. 10 (2019) 2521, https://doi.org/10.1038/s41467-019-10524-2.

[56] A. Fujishima, X. Zhang, D.A. Tryk, TiO_2 photocatalysis and related surface phenomena, Surf. Sci. Rep. 63 (2008) 515–582, https://doi.org/10.1016/j.surfrep.2008.10.001.

[57] O.E. Dagdeviren, D. Glass, R. Sapienza, E. Cortés, S.A. Maier, I.P. Parkin, P. Grütter, R. Quesada-Cabrera, The effect of photoinduced surface oxygen vacancies on the charge carrier dynamics in TiO_2 films, Nano Lett. 21 (2021) 8348–8354, https://doi.org/10.1021/acs.nanolett.1c02853.

[58] M. Luna, M. Barawi, S. Gómez-Moñivas, J. Colchero, M. Rodríguez-Peña, S. Yang, X. Zhao, Y.H. Lu, R. Chintala, P. Reñones, V. Altoe, L. Martínez, Y. Huttel, S. Kawasaki, A. Weber-Bargioni, V.A. de la Peña O'Shea, P. Yang, P.D. Ashby, M. Salmeron, Photoinduced charge transfer and trapping on single gold metal nanoparticles on TiO_2, ACS Appl. Mater. Interfaces 13 (2021) 50531–50538, https://doi.org/10.1021/acsami.1c13662.

[59] M. Macias-Montero, C. Lopez-Santos, A.N. Filippin, V.J. Rico, J.P. Espinos, J. Fraxedas, V. Perez-Dieste, C. Escudero, A.R. Gonzalez-Elipe, A. Borras, In situ determination of the water condensation mechanisms on superhydrophobic and superhydrophilic titanium dioxide nanotubes, Langmuir 33 (2017) 6449–6456, https://doi.org/10.1021/acs.langmuir.7b00156.

[60] K. Chandrasekaran, J. Thomas, Photochemical reduction of carbonate to formaldehyde on TiO_2 powder, Chem. Phys. Lett. 99 (1983) 7–10.

[61] J.Y.Y. Loh, N.P. Kherani, X-ray photospectroscopy and electronic studies of reactor parameters on photocatalytic hydrogenation of carbon dioxide by defect-laden indium oxide hydroxide nanorods, Molecules 24 (2019) 1–11, https://doi.org/10.3390/molecules24213818.

[62] M. Morikawa, N. Ahmed, Y. Yoshida, Y. Izumi, Photoconversion of carbon dioxide in zinc–copper–gallium layered double hydroxides: The kinetics to hydrogen carbonate and further to CO/methanol, Appl. Catal. B Environ. 144 (2014) 561–569, https://doi.org/10.1016/j.apcatb.2013.07.065.

[63] H. Park, H.-H. Ou, A.J. Colussi, M.R. Hoffmann, Artificial photosynthesis of C1–C3 hydrocarbons from water and CO_2 on titanate nanotubes decorated with nanoparticle elemental copper and CdS quantum dots, J. Phys. Chem. A 119 (2015) 4658–4666, https://doi.org/10.1021/jp511329d.

[64] L. Yuliati, H. Yoshida, Photocatalytic conversion of methane, Chem. Soc. Rev. 37 (2008) 1592–1602.

[65] Y. Shiraishi, S. Kanazawa, D. Tsukamoto, A. Shiro, Y. Sugano, T. Hirai, Selective hydrogen peroxide formation by titanium dioxide photocatalysis with benzylic alcohols and molecular oxygen in water, ACS Catal. 3 (2013) 2222–2227, https://doi.org/10.1021/cs400511q.

[66] Z.W. Wang, Q. Wan, Y.Z. Shi, H. Wang, Y.Y. Kang, S.Y. Zhu, S. Lin, L. Wu, Selective photocatalytic reduction CO_2 to CH_4 on ultrathin TiO_2 nanosheet via coordination activation, Appl. Catal. B Environ. 288 (2021) 120000–120008, https://doi.org/10.1016/j.apcatb.2021.120000.